International Journal of Control, Automation and Systems 16(2) (2018) 769-781
http://dx.doi.org/10.1007/s12555-016-0488-6
ISSN:1598-6446 eISSN:2005-4092
http://www.springer.com/12555

Realization and Demonstration of Enhanced Korean High-speed Train Navigation System with Noise Filtering Schemes

Hyunwoo Ko, Youngbo Shim, and Seung-Hyun Kong*

Abstract: A precise train navigation system for Korean high-speed trains having a maximum speed of 400km/h or higher was developed in 2015. The navigation system employs multi-sensor fusion technique, and until now, the target performance of 1-meter instantaneous positioning accuracy in all environments including the Global Positioning System (GPS)-denied environments such as tunnels has been demonstrated using only simulations for various scenarios. In this paper, we demonstrate that the train navigation system achieves the target positioning accuracy in real train environments, which is the first train navigation system that the performance of sub-meter accuracy is demonstrated with real data in the literature. We also introduce additional filtering schemes applied to the various sensors of the train navigation system to enhance the sensor data corrupted by large unexpected noises often observed in the train environments. The train navigation system is properly modified for real train environments to employ the filtering schemes.

Keywords: Global positioning system, high-speed train, inertial navigation system, navigation, noise filtering, sensor fusion.

1. INTRODUCTION

Accurate position information of a train is a vital component for the efficiency, safety, and convenience of the train-based transportation systems. In practice, it is used for maintenance, safety equipment, train control, monitoring, and other various applications [1, 2]. For instance, as safety becomes important, automatic train control (ATC) systems require accurate, precise, and reliable position of a train in operation. In addition, a rail inspection trains require accurate instantaneous location to tag a maintenance location of the rail. However, in practice, accurate location of a train is not always available with global positioning system (GPS) because there are train environments where GPS is degraded or denied [3].

Recently, a train navigation system focuses on vehicle-based system instead of track-based system. In general, conventional track-based system implements navigation sensors or devices on the tracks (or rails), but the positioning accuracy is quite poor. For an accurate position information, navigation sensors and systems [4, 5], which are used in aviation, marine, military, are adopted to the train-based transportation systems. U.S. and Europe have already developed next-generation train navigation systems utilizing GPS, inertial navigation system (INS), radio frequency identification (RFID), and various sensors by integrating Kalman filter (KF) based navigation filters, which have performed a few-meter level positioning accuracy [6].

Multi-sensor fusion based navigation filters have been studied for decades. In the studies, KF based recursive filters, e.g, KF for linear systems, extended KF (EKF) and unscented KF (UKF) for nonlinear systems, have been widely used, because they provide (exact or near) optimal estimation results and they are easily applicable to broad range of navigation problems [7–9]. However, KF-based filters have degraded estimation performance for unexpected errors (outliers) [10]. Particle filter (PF) can provide accurate estimation result in highly nonlinear system from non-Gaussian errors but have sample impoverishment and high computational cost issue [11]. Recursive filters are often called infinite impulse response (IIR) filter, and IIR filters have disadvantages of accumulation of errors from utilizing their past input and output [12]. To overcome shortages of IIR filters, many finite impulse response (FIR) filters that do not have a feedback are studied recently for robust state estimation [13, 14].

To reduce the performance degradation from sensor failures and unexpected large errors, a number of studies have focused on fault monitoring and detection problems. In addition, for estimation problems with complex and nonlinear system models, data-based fault diagnosis

Manuscript received August 4, 2016; revised March 29, 2017 and August 2, 2017; accepted September 18, 2017. Recommended by Associate Editor Gon-Woo Kim under the direction of Editor Euntai Kim. This work (2013R1A2A2A01067863) was supported by Mid-career Researcher Program through NRF grant funded by the Korean government (MEST).

Hyunwoo Ko, Youngbo Shim, and Seung-Hyun Kong are with the CCS Graduate School for Green Transportation at the Korea Advanced Institute of Science and Technology (KAIST), Daejeon 305-701, Korea (e-mails: {kohyunwoo, shim36145, skong}@kaist.ac.kr).
* Corresponding author.

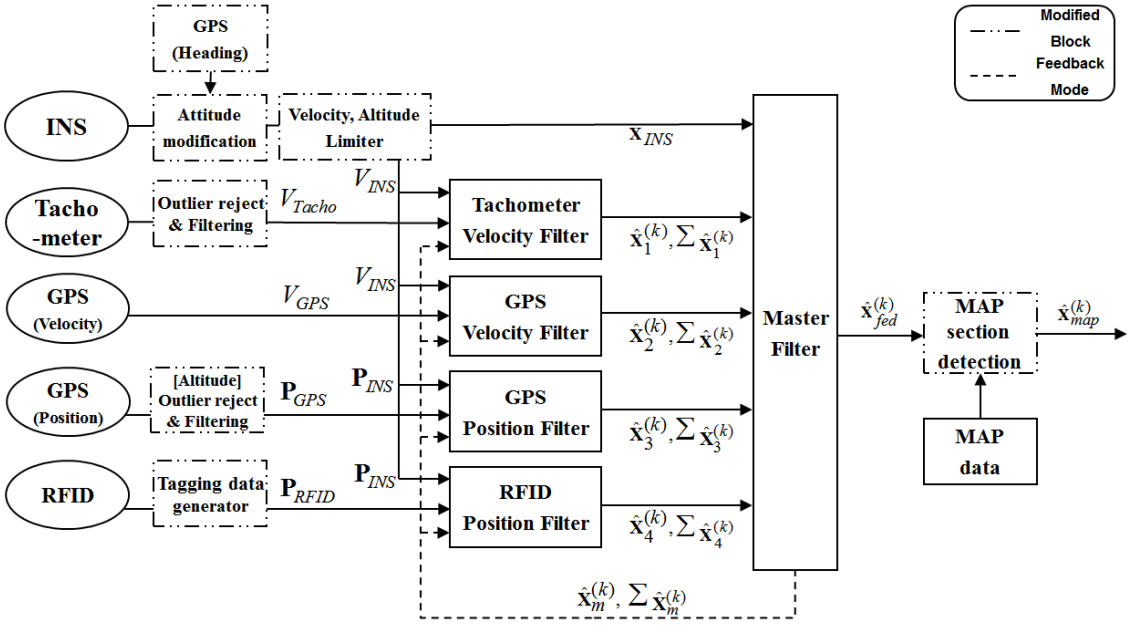

Fig. 1. Structure of the Korean high-speed train navigation system.

has gained more attention than conventional model-based fault diagnosis (i.e., KF-based) [15]. For example, GPS receiver autonomous integrity monitoring (RAIM) techniques deal with rejecting statistical outliers in the GPS measurements [16], principal component analysis (PCA) is utilized for electrocardiography (ECG) signal detection [17], and information sharing factor (ISF) is adopted to determine GPS constellation in vehicular environments [18] and to detect slip and slide errors in the high-speed train (HST) [19].

A HST HEMU-430X has been developed to offer a speed over 400km/h by Korean Railroad Research Institute (KRRI) and Hyundai Rotem Inc. To accomplish a target 1-meter positioning accuracy (which is top tier accuracy in the world), the train navigation system employing multi-sensor data fusion and map matching algorithm was introduced [20]. It utilizes GPS, inertial measurement unit (IMU), tachometer, RFID, and it is designed using federated Kalman filter (FKF) [21].

However, there have been a number of useful filter techniques different from FKF introduced in the literature, for example, PF, FIR, and measurement fusion (MF) techniques. And it is found that the MF technique can produce a better estimation performance than the state vector fusion (SVF) such as FKF [22, 23], and the MF technique can be employed in the HST navigation system [20]. However, the HST navigation system [20] employs the FKF, because the FKF has a lower computational cost than the centralized KF (CKF) with MF and it is easy to monitor a sensor failure. In fact, the HST navigation system with FKF [20] achieves a high estimation accuracy due to the enough sensor measurements which are not only accurate but also frequent such as GPS and RFID. Kim *et al.* [19] proposed HST navigation system robust to tachometer sensor failure in 2015, employing feedback scheme with information sharing (IS) approach. This HST navigation system has been developed in 7∼8 technology readiness level (TRL) phase, thus, we have to consider computational complexity and costs.

In this paper, we devise a real-time navigation systems for high speed trains utilizing the theoretical algorithm [20], and modify the algorithm for unexpected sensor measurements due to the various noises. In addition, we demonstrate that the train navigation system employing multiple sensors significantly improves the positioning accuracy (1-meter Circular Error Probability (CEP)) over the conventional train navigation system during GPS outages. Since disclosing a research in TRL 7∼8 level of development phase is rare in high speed train navigation systems and the navigation errors observed in the train environments are often unexpected in the development of theoretical algorithms, this work provides one of the first field demonstration, empirical error observation analysis, and modifications to the theoretical algorithm of the navigation systems for high-speed trains. To the best of our knowledge, there are a number of studies to achieve high positioning and navigation accuracy for high-speed trains in Europe and China [24, 25], however, their performances have been demonstrated only by simulations, but there has been no field demonstration and no analysis to discuss the difference between the theoretical algorithm and practical algorithm modifications and issues in the real high-speed trains. We believe this paper is helpful for readers who are interested with sensor data processing and multisensor-

fusion based system, since the paper deals with practical issues such as data drop and unexpected sensor noise rejection. The proposed system in this paper is applicable to nonlinear systems using multiple sensor inputs, for example, the proposed system is suitable to decentralized networked systems receiving sensor measurements from multiple points [26].

The rest of this paper is organized as follows. In Section 2, HST navigation system is briefly introduced. In Section 3, we introduce details of realization process and signal processing techniques. We demonstrate our realized system with filed data in Section 4 and give conclusion in Section 5.

2. NAVIGATION SYSTEM

A multi-sensor based navigation system for Korean HST is designed in 2015, based on a FKF for the low computational cost and easy implementation of fault detection scheme. Theoretically, the system may be divided into three parts (i.e., local and master filters, and map matching) [20]. The recent structure of the Korean HST navigation system is illustrated in Fig. 1 where the filter and map matching blocks with solid lines are designed in 2015. During the realization and demonstration phases, modified blocks with dashed dots are added to deal with unexpected errors. In this section, we briefly introduce the train navigation algorithm which is previously designed in [20, 27], and focus on data analysis from realization and demonstration perspectives in section 3 We devise a real-time navigation system for the HST utilizing the theoretical algorithm [20], and modify the algorithm for unexpected measurement erorrs due to the various noises.

The navigation system uses INS as a reference for the algorithm and three other sensors, GPS, tachometer, and RFID for measurements. The GPS sensor provides position and velocity information in open-sky conditions, tachometer provides velocity of the train, and RFID receiver reads accurate positions of RFID tags on the rails.

Note that, sensor measurements are independent each other because of their own measurement schemes. The GPS position and velocity estimates are independent since the GPS position is determined by the code phase measurements while the GPS velocity is measured utilizing the Doppler frequency observations of the GPS signals. We use raw measurements of IMU such as angular velocity and acceleration from gyroscope and accelerometer, respectively. Also, tachometer counts encoder pulses measured in a rotating wheel and RFID reader receives known positions of RFID tags along the rails. Each sensor measurement is processed by their own local filter, and then local filter outputs are integrated in the master filter.

The master filter provides a federated output and feedbacks. In [20], HST navigation filter does not employ a feedback scheme, however in this paper, feedback scheme is chosen for correction of each local filters. In the realization phase, entire local filters are corrected by the master filter output, otherwise, those local filters diverge due to the accumulation of errors at GPS outages and slip (or slide) environments. Note that, the estimates of the local filters are mutually independent and there exists no correlation when the initial states of local filters are uncorrelated with each other [28].

However, in practice, there can be cross-correlation terms in the noise covariance matrix. Carlson proposes an upper bound matrix to resolve the cross-correlation problem [28], and, exploiting the concept of the upper bound matrix, we adopt a diagonal tuning matrix to weight the diagonal covariance matrix. The diagonal terms in the tuning matrix are determined by considering the performance of the HST navigation system observed in the real field. Finally, the master filter output is revised by the map matching algorithm.

2.1. Local filter

2.1.1 System model

The system model of the navigation system is an INS error model which is derived from general INS navigation equations using perturbation method [27]. The system model is found as

$$\delta\dot{\mathbf{x}}^{(k)} = F_{INS}^{(k)}\delta\mathbf{x}^{(k)} + W^{(k)}\mathbf{w}^{(k)}, \tag{1}$$

where $(\cdot)^{(k)}$ denotes vector or value at k-th time instant. Also, δ is the error vector, $\mathbf{x}$ is the state vector, F_{INS} is the system matrix derived from general INS equations [27], W is the system noise matrix of $\mathbf{w}$, and $\mathbf{w}$ has zero mean Gaussian distribution. The error state vector $\delta\mathbf{x}$ and noise vector $\mathbf{w}$ are defined as

$$\delta\mathbf{x} = \left[\ \delta\mathbf{P}\ \ \delta V^n\ \ \delta\mathbf{Q}_b^n\ \ \nabla\ \ \eta\ \right]^T, \tag{2a}$$

$$\mathbf{w} = \left[\ \mathbf{w}_a\ \ \mathbf{w}_g\ \right]^T, \tag{2b}$$

where $\mathbf{P} = [L\ l\ h]$ is the position vector ([Latitude, longitude, height]), $\boldsymbol{V}^n = [V_N\ V_E\ V_D]$ is the velocity vector in north-east-down (NED) directions (where superscript n denotes navigation frame), $\mathbf{Q}_b^n = [q_0\ q_1\ q_2\ q_3]$ is the quaternion vector for attitude, $\nabla = [\nabla_X\ \nabla_Y\ \nabla_Z]$ is the accelerometer bias error vector in x,y,z-direction of body frame, $\eta = [\eta_x\ \eta_y\ \eta_z]$ is the gyroscope error vector in x,y,z- direction of body frame. Accelerometer noise vector $\mathbf{w}_a = [w_{ax}\ w_{ay}\ w_{az}]$ and gyroscope noise vector $\mathbf{w}_g = [w_{gx}\ w_{gy}\ w_{gz}]$ have zero-mean Gaussian distributions with covariance matrices $\mathbf{\Lambda}_a = diag([\sigma_{a_x}^2\ \sigma_{a_y}^2\ \sigma_{a_z}^2])$ and $\mathbf{\Lambda}_g = diag([\sigma_{g_x}^2\ \sigma_{g_y}^2\ \sigma_{g_z}^2])$, respectively, where $diag(\cdot)$ and σ denote diagonal matrix function and one standard deviation of a noise, respectively. Utilizing a tuning matrix $\mathbf{\Gamma}$, the overall noise covariance matrix Λ is defined as

$$\mathbf{\Lambda} = \mathbf{\Gamma}\begin{bmatrix} \mathbf{\Lambda}_a & O_{3\times3} \\ O_{3\times3} & \mathbf{\Lambda}_g \end{bmatrix}, \tag{3a}$$

$$\Gamma = diag\left(\begin{bmatrix} \gamma_a & \gamma_a & \gamma_a & \gamma_g & \gamma_g & \gamma_g \end{bmatrix}\right), \tag{3b}$$

where γ_a and γ_g are weighting factors for accelerometer and gyroscope noises, respectively. Note that the weighting factors need to be determined considering the navigation performance in the real environments. The system matrix F_{INS} and noise matrix W can be found in [20, 27].

2.1.2 Measurement model

GPS position and velocity, tachometer velocity, and RFID position are measured according to their update rate. Since the system model is derived base on the error model [27], the measurements are expressed as

$$\zeta^{(k)}_{GPS\_P} = \mathbf{P}_{INS} - \mathbf{P}_{GPS} = H_{GPS\_P}\delta\mathbf{x}^{(k)} + \mathbf{v}^{(k)}_{GPS\_P}, \tag{4a}$$
$$\zeta^{(k)}_{GPS\_V} = \boldsymbol{V}_{INS} - \boldsymbol{V}_{GPS} = H_{GPS\_V}\delta\mathbf{x}^{(k)} + \mathbf{v}^{(k)}_{GPS\_V}, \tag{4b}$$
$$\zeta^{(k)}_{Tacho} = C^b_n\boldsymbol{V}^n_{INS,x} - \boldsymbol{V}^b_{Tacho,x} = H_{Tacho}\delta\mathbf{x}^{(k)} + \mathbf{v}^{(k)}_{Tacho}, \tag{4c}$$
$$\zeta^{(k)}_{RFID} = \mathbf{P}_{INS} - \mathbf{P}_{RFID} = H_{RFID}\delta\mathbf{x}^{(k)} + \mathbf{v}^{(k)}_{RFID}, \tag{4d}$$

where ζ_{GPS_P}, ζ_{GPS_V}, ζ_{Tacho}, and ζ_{RFID} are measurements of GPS position, GPS velocity, tachometer velocity, and RFID position, respectively. Also, $\mathbf{P}_{INS}$, $\mathbf{P}_{GPS}$, $\mathbf{P}_{RFID}$, $\boldsymbol{V}_{INS}$, $\boldsymbol{V}_{GPS}$, $\boldsymbol{V}^n_{INS,x}$, and $\boldsymbol{V}^b_{Tacho,x}$ are position and velocity vectors of INS, GPS, tachometer and RFID. The quantity C^b_n represents the coordinate transformation matrix from the body frame to the navigation frame. Measurement noise vectors $\mathbf{v}_{GPS\_P}, \mathbf{v}_{GPS\_V}, \mathbf{v}_{Tacho}$, and $\mathbf{v}_{RFID}$ have zero-mean Gaussian distributions with covaricance matrices $\mathbf{R}_{GPS\_P}, \mathbf{R}_{GPS\_V}, \mathbf{R}_{Tacho}$, and $\mathbf{R}_{RFID}$, respectively. In particular, velocity vectors $\boldsymbol{V}^n_{INS,x}$ and $\boldsymbol{V}^b_{Tacho,x}$ for tachometer model, use only values in x-direction of the navigation frame and the body frame, respectively (where superscript n and b denote navigation frame and body frame, subscript x denotes x-direction component), because tachometer only provides one-dimensional velocity in the heading direction of train. The measurement matrices H_{GPS_P}, H_{GPS_V}, H_{Tacho}, and H_{RFID} are found as

$$H_{GPS\_P} = \begin{bmatrix} 1 & 0 & 0 & O_{1\times 13} \\ 0 & 1 & 0 & O_{1\times 13} \\ 0 & 0 & 1 & O_{1\times 13} \end{bmatrix}, \tag{5a}$$
$$H_{GPS\_V} = \begin{bmatrix} O_{1\times 3} & 1 & 0 & 0 & O_{1\times 10} \\ O_{1\times 3} & 1 & 0 & 0 & O_{1\times 10} \\ O_{1\times 3} & 1 & 0 & 0 & O_{1\times 10} \end{bmatrix}, \tag{5b}$$
$$H_{Tacho} = \begin{bmatrix} O_{1\times 3} \mid C^b_n(1,:) \mid H_s(1,:) \mid O_{1\times 6} \end{bmatrix}, \tag{5c}$$
$$H_{RFID} = \begin{bmatrix} 1 & 0 & 0 & O_{1\times 13} \\ 0 & 1 & 0 & O_{1\times 13} \\ 0 & 0 & 1 & O_{1\times 13} \end{bmatrix}, \tag{5d}$$

where submatrix H_s in (5c) and the derivations for the expressions in (4), (5) can be found in [20].

2.1.3 State estimation

Each local filter is based on a Kalman filter in the considered HST navigation system. Based on the system and measurement model equations, the Kalman filter in the i-th local filter computes the error state vector $\delta\hat{\mathbf{x}}^{(k)}_i$ which is then subtracted from the INS state $\mathbf{x}^{(k)}_{INS}$ to produce the local filter output $\hat{\mathbf{x}}^{(k)}_i$ as

$$\hat{\mathbf{x}}^{(k)}_i = \mathbf{x}^{(k)}_{INS} - \delta\hat{\mathbf{x}}^{(k)}_i. \tag{6}$$

2.2. Master filter

Local filter outputs are integrated by a master filter. The master filter equations are shown in [20] as

$$\hat{\mathbf{x}}^{-(k)}_m = f\left(\hat{\mathbf{x}}^{(k-1)}_m\right), \tag{7}$$
$$\Sigma_{\hat{\mathbf{x}}^{-(k)}_m} = \Phi^{(k,k-1)}\Sigma_{\hat{\mathbf{x}}^{(k-1)}_m}\Phi^{(k,k-1)T} + \ldots + W^{(k)}\Lambda^{(k)}W^{(k)T}, \tag{8}$$
$$\left(\Sigma_{\hat{\mathbf{x}}^{(k)}_m}\right)^{-1} = \sum_{i=1}^{4}\left(\Sigma_{\hat{\mathbf{x}}^{(k)}_i}\right)^{-1}, \tag{9}$$
$$\hat{\mathbf{x}}^{(k)}_m = \Sigma_{\hat{\mathbf{x}}^{(k)}_m}\left[\sum_{i=1}^{4}\left(\Sigma_{\hat{\mathbf{x}}^{(k)}_i}\right)^{-1}\hat{\mathbf{x}}^{(k)}_i\right], \tag{10}$$

where $f(\cdot)$, $\hat{\mathbf{x}}^{-(k)}_m$, $\Sigma_{\hat{\mathbf{x}}^{-(k)}_m}$, $\hat{\mathbf{x}}^{(k)}_m$, $\Sigma_{\hat{\mathbf{x}}^{(k)}_m}$, and $\Sigma_{\hat{\mathbf{x}}^{(k)}_i}$ represent the nonlinear navigation system function, master filter a priori state estimation and covariance, master filter state estimation and covariance, and i-th local filter covariance, respectively. The transition matrix of the system is defined as

$$\Phi^{(k,k-1)} = e^{F_{INS}\left(t^{(k)} - t^{(k-1)}\right)}. \tag{11}$$

The master filter output is also written as federated output $\hat{\mathbf{x}}^{(k)}_{fed}$ in this paper.

2.3. Map matching

For the best performance of positioning accuracy, map matching algorithm is additionally applied to the FKF structure. Mostly, a small interval between two map points on a rail can be considered as a straight line because rails for HST have small curvatures at the corners. Utilizing this idea, [20] adopts a simple projection method which finds two map points ($\alpha^{(k)}$ and $\beta^{(k)}$) nearby a position $\hat{\mathbf{P}}^{(k)}_m$ (from master filter output $\hat{\mathbf{x}}^{(k)}_m$) and it projects $\hat{\mathbf{P}}^{(k)}_m$ to a vector $\overrightarrow{\alpha^{(k)}\beta^{(k)}}$. A projection equation is expressed as

$$proj\left(\overrightarrow{\alpha^{(k)}\hat{\mathbf{P}}^{(k)}_m}, \overrightarrow{\alpha^{(k)}\beta^{(k)}}\right) = \left(\frac{\overrightarrow{\alpha^{(k)}\hat{\mathbf{P}}^{(k)}_m} \cdot \overrightarrow{\alpha^{(k)}\beta^{(k)}}}{\left|\overrightarrow{\alpha^{(k)}\beta^{(k)}}\right|^2}\right) \cdot \overrightarrow{\alpha^{(k)}\beta^{(k)}}, \tag{12}$$

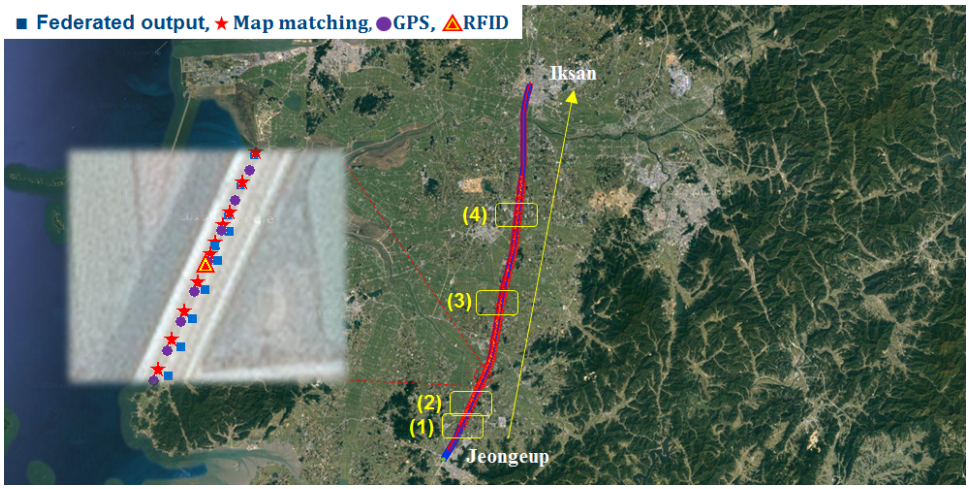

Fig. 2. Testbed Map: Jeongeup station to Iksan station.

Table 1. Acquired data list used in the navigation algorithm.

Sensor	Data	Description	Unit	Update Period
GPS (Novatel OEM 628™)	Time	GPS time	[ms]	10Hz
	Position	Latitude, longitude, height	[deg, deg, m]	
	Velocity	Driving Speed (1-dimensional)	[m/s]	
	Heading	Heading angle of the train reference to the north	[deg]	
	Signal quality	0: Proper signal condition 1: Improper signal condition (i.g., GPS outages)	integer	
IMU (ADIS16488)	Time	IMU iteration time	[ms]	200Hz
	Gyroscope	Angular velocity (roll, pitch, yaw)	[deg/s]	
	Acceleration	Acceleration (x,y,z)	[g]	
Tachometer (PHS-6C)	Encoder counts	Transformed to speed of the train	[m/s]	200Hz
RFID	Position	RFID tag position (Llh)	[deg, deg, m]	Train tagging time (Not periodic)

then map matching result $\hat{\mathbf{P}}_{map}^{(k)}$ is computed as

$$\hat{\mathbf{P}}_{map}^{(k)} = proj\left(\overrightarrow{\alpha^{(k)}\hat{\mathbf{P}}_{m}^{(k)}}, \overrightarrow{\alpha^{(k)}\beta^{(k)}}\right) + \alpha^{(k)}. \tag{13}$$

3. ACQUISITION AND PROCESSING OF FIELD NAVIGATION DATA

3.1. Experiment overview

3.1.1 Testbed information

A testbed of the HST navigation system is set between Jeongeup station and Iksan station about 41km length railroad, and it is illustrated in Fig. 2. On the testbed, 94 numbers of RFID tags are installed on rails with three tunnels which range from 250m to 600m. In the testbed, map points' latitude values have the largest variation compared to longitude and height values because rails are biased in latitude direction.

3.1.2 Descriptions of train driving experiment

Three sensors, GPS, IMU, and tachometer, were attached to the HST except for RFID tag receiver because of its incomplete development. The HST stopped for several dozen minutes at the Gwangju station (Lat. 35.13952833^o, lon.126.7903667^o). During the static state of the train, sensors were initialized and stabilized. After the preparation time, the train started to move, and it passed Jeongeup station without a stop. All sensor measurements were recorded with their own update rate until the train arrived at Iksan station. Navigation data was recorded from Gwangju station to Iksan station, but the HST navigation algorithm was demonstrated from the Jeongeup station because RFID tags and map data were only available on the testbed. Acquired sensor data are summarized on Table 1. The HST algorithm rate is set to 10Hz as same as GPS update rate to fit the slowest measurement update.

3.2. Navigation data processing

Before realization and demonstration of this HST navi-

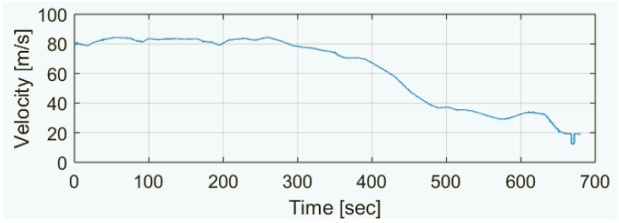

(a) GPS velocity raw measurement.

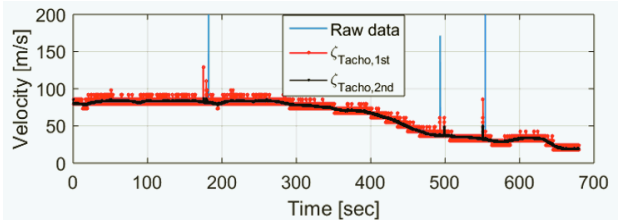

(b) Tachometer raw (blue), 1st outlier rejected (red), and 2nd moving average filtered (black) measurements.

Fig. 3. GPS and tachometer velocity measurements.

gation system, sensor measurements should be evaluated. Since this HST navigation filter is not IIR based filter but KF based structure (i.e., FKF), error distribution of each sensor are assumed as additive white Gaussian distribution. However, HST driving environments are seriously tough environments due to GPS-denied condition (i.e., tunnel), unique train vibrations, slip and sliding of wheels, and unstable train power source. Thus, navigation sensor measurements are easy to be distorted from various noise sources including statistical outliers. We could not abandon aforementioned benifits of FKF, thus, we try to remove the noises utilizing data processing and algorithm optimization approches. Here, issues which frequently appear in realization of navigation system are introduced to be figured out.

3.2.1 Data drop

In realistic environments, we found that GPS data (as shown in Table 1) are dropped for a few seconds aperiodically. During data drop period, any GPS data are not recorded. If GPS data drop is ignored, GPS data will not be synchronized with other data such as IMU or tachometer. This unsynchronization leads divergence of navigation result. Thus, GPS time interval should be checked in every update instance whether it is more than 100ms (10Hz GPS update rate), and the dropped vacant data place should be filled by redundant terms (i.e., zero matrices) which has a size of dropped time interval. These redundant terms will not be computed for state update in GPS local filters (i.e., GPS position and velocity) but only covariances in local filters will be time propagated.

3.2.2 Tachometer velocity

Tachometer sensor is vulnerable to wheel slip and slide according to railroad conditions [20]. Slip and slide of the wheel lead continuous small errors or sudden large errors. Here, tachometer velocity measurements have large errors like impulse noises as shown in Fig. 3(b). Also, additional noises from driving vibration and unstable power source distort tachometer velocity measurements. In [19], Kim *et al* propose a slip and slide detection (SSD) algorithm using an information sharing method, which is to prevent the significant performance degradation due to the tachometer failure in the feedback scheme. However, in this paper, the SSD algorithm is not adopted because it requires two stage FKF structure and information sharing algorithm. In the realization phase of the HST navigation system, we propose and apply simple outlier rejection and digital filtering techniques to the sensor measurements to reduce computational cost produce and to produce valid input to the local filters.

To reduce effects of various noises, outliers (impulse like noises) which considered as slip and slide errors are removed preferentially before utilizing moving average filtering. The outliers of tachometer velocity measurements can be removed by comparison with GPS velocity measurements as a reference. Because GPS velocity measurements are measured simultaneouly with tachometer measurements and considered very accurate [29]. As shown in Fig. 3(a), GPS velocity measurements less suffer from noises than tachometer velocity measurements. The mean μ_{GPS_V} and standard deviation (std.) σ_{GPS_V} of the GPS velocity measurements are computed as

$$\mu_{GPS\_V} = \frac{1}{K}\sum_{k=1}^{K} \zeta_{GPS\_V}^{(k)}, \tag{14a}$$

$$\sigma_{GPS\_V} = \sqrt{\frac{1}{K}\sum_{k=1}^{K} \left(\zeta_{GPS\_V}^{(k)} - \mu_{GPS\_V}\right)^2}, \tag{14b}$$

where K represents the data size of GPS velocity measurements. Tachometer velocity measured at k-th time instant $\zeta_{Tacho}^{(k)}$ can be detected as an outlier if a difference between $\zeta_{Tacho}^{(k)}$ and μ_{GPS_V} is larger than twice of std. of GPS velocity σ_{GPS_V}. The outlier $\zeta_{Tacho}^{(k)}$ is replaced by the median result $\zeta_{Tacho,med}^{(k)}$ with median size of M [30] as

$$\zeta_{Tacho,1st}^{(k)} = \begin{cases} \zeta_{Tacho,med}^{(k)} & \text{if } |\zeta_{Tacho}^{(k)} - \mu_{GPS\_V}| > 2\sigma_{GPS\_V} \\ \zeta_{Tacho}^{(k)} & \text{if } |\zeta_{Tacho}^{(k)} - \mu_{GPS\_V}| < 2\sigma_{GPS\_V}. \end{cases} \tag{15}$$

We found a proper value of M experimentally as 21. Note that, 21 numbers of tachometer measurements takes about 0.1 seconds (considering 200Hz tachometer update rate), and it matches HST navigation algorithm rate. After removing outliers, a moving average filter is applied as

$$\zeta_{Tacho,2nd}^{(k)} = \zeta_{Tacho,2nd}^{(k-1)} + \frac{\zeta_{Tacho,1st}^{(k-1)} + \zeta_{Tacho,1st}^{(k)}}{N}, \tag{16}$$

where N is a filtering window size, and it is set to 11 experimentally. Fig. 3(b) shows raw and filtered data.

3.2.3 GPS altitude

The main noise of GPS altitude (height) measurement is an impulse noise at the GPS outages. As shown in Fig. 4, impulse noises of the GPS altitude measurements appear when the quality of the GPS signal is bad (GPS indicator represents signal quality: 0 for good and 1 for bad in Fig. 4(b)). Same process of the outlier and noise removals on the tachometer velocity measurements using equations (14) to (16) is applied to reduce the noise in the GPS altitude measurements. The mean μ_{GPS_Al} and standard deviation σ_{GPS_Al} of the GPS altitude measurements are computed as

$$\mu_{GPS\_Al} = \frac{1}{K}\sum_{k=1}^{K} \zeta_{GPS\_Al}^{(k)}, \tag{17a}$$

$$\sigma_{GPS\_Al} = \sqrt{\frac{1}{K}\sum_{k=1}^{K} \left(\zeta_{GPS\_Al}^{(k)} - \mu_{GPS\_Al}\right)^2}. \tag{17b}$$

The outliers of the GPS altitude measurements are detected and removed in the same way as

$$\zeta_{GPS\_Al,1st}^{(k)} = \begin{cases} \zeta_{GPS\_Al,med}^{(k)} \\ \quad \text{if } |\zeta_{GPS\_Al}^{(k)} - \mu_{GPS\_Al}| > 2\sigma_{GPS\_Al}, \\ \zeta_{GPS\_Al}^{(k)} \\ \quad \text{if } |\zeta_{GPS\_Al}^{(k)} - \mu_{GPS\_Al}| < 2\sigma_{GPS\_Al}, \end{cases} \tag{18}$$

where 21 $(M = 21)$ consecutive numbers of GPS altitude measurements are collected to calculate a median value $\zeta_{GPS\_Al,med}^{(k)}$ for replacing an outlier. Removing outliers, the final output of GPS altitude $\zeta_{GPS\_Al,2nd}^{(k)}$ is computed by employing a moving average filter, similar to (16).

The idea of outlier detection applied to the HST navigation system can be found in various areas such as GPS receiver autonomous integrity monitoring (RAIM) techniques [16] and electrocardiogram (ECG) signal processing techniques [17]. We adopt simple idea of the outlier rejection in [16, 17], even though it is not exactly same way. This simple idea is enough to detect and remove outliers since the outliers in the tachometer velocity and GPS altitude have much larger values than the normal values. The results of tachometer velocity and GPS altitude measurements after outlier and noise rejection are shown in the Fig. 3(b) and 4(a).

3.2.4 RFID virtual measurement

RFID measurement is not included in the field data because the development of RFID module has not been completed. The RFID module is a key component in this system because it enables accurate positioning in GPS-denied environments. Thus, we have to generate virtual RFID

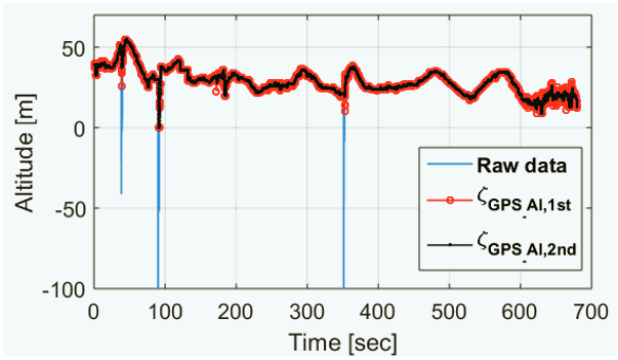

(a) GPS altitude (blue), 1st outlier rejected (red), and 2nd moving average filtered (black) measurements.

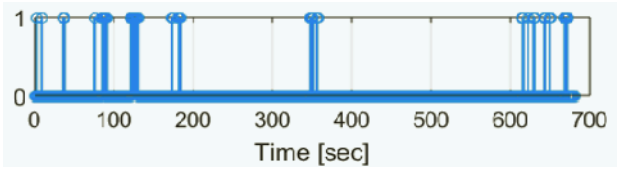

(b) GPS signal quality indicator: 0 for Good, 1 for Bad.

Fig. 4. GPS altitude and signal quality measurements.

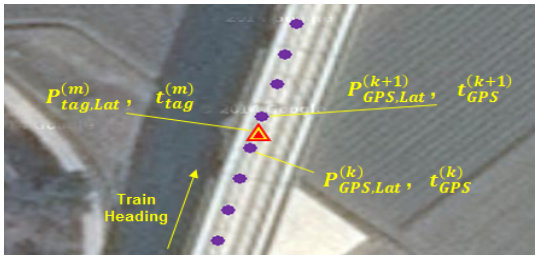

Fig. 5. Geometry of RFID tag (triangles) and GPS positions (dots).

tagging data to realize the HST navigation system and demonstrate its performance. As shown in Fig. 5, a RFID tag is located between GPS position results of the train. Note that, it is also placed to satisfy the location accuracy of the train specified for the Balise in [31]. Using time information of two GPS positions, an instant time when the train passes on the m-th RFID tag can be estimated as

$$t_{tag}^{(m)} = \frac{\mathbf{P}_{tag,Lat}^{(m)} - \mathbf{P}_{GPS,Lat}^{(k)}}{\mathbf{P}_{GPS,Lat}^{(k+1)} - \mathbf{P}_{GPS,Lat}^{(k)}} \times \Delta t_{GPS} + t_{GPS}^{(k)}, \tag{19}$$

where $\mathbf{P}_{tag,Lat}^{(m)}$, $\mathbf{P}_{GPS,Lat}^{(k)}$, Δt_{GPS}, and $t_{GPS}^{(k)}$ are latitude of m-th RFID tag, latitude of GPS position at time k, time interval of GPS time, and GPS time at time k, respectively.

3.2.5 IMU gyroscope and accelerometer

IMU sensor provides acceleration from the accelerometer and angular velocity from the gyroscope in x, y, z-directions of the body frame. Because the body is a

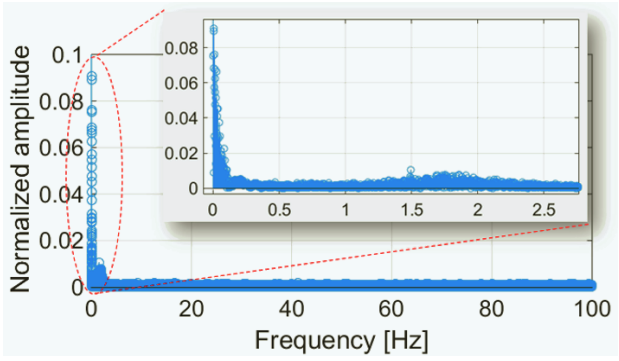

(a) Gyroscope z-direction (yaw-rate).

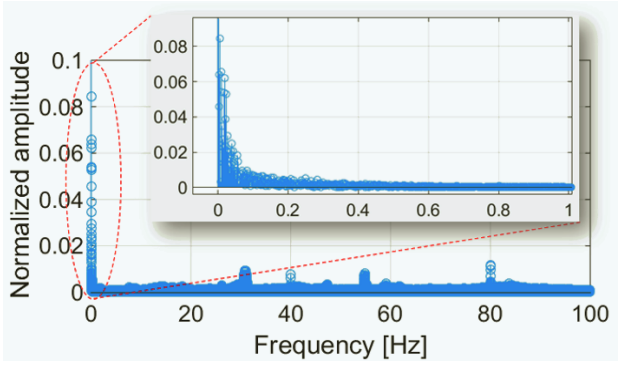

(b) Acceleration x-direction (train heading direction).

Fig. 6. Examples of positive FFT results.

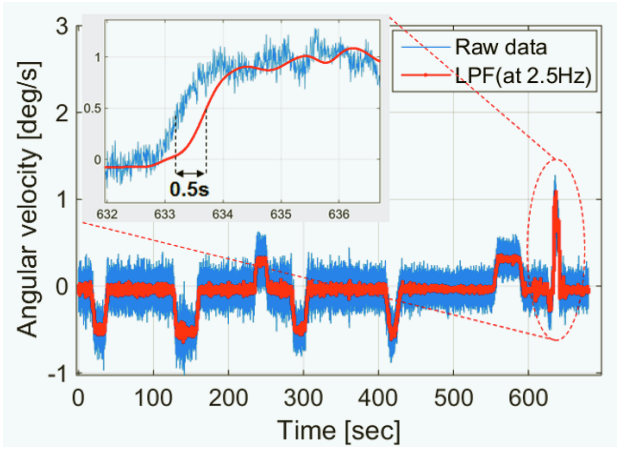

(a) Gyroscope z-direction (yaw-rate).

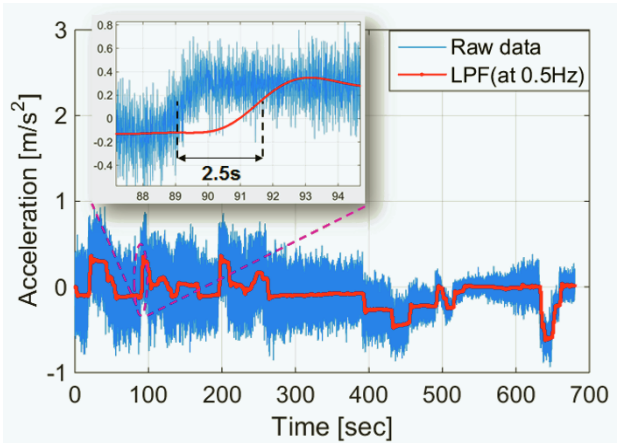

(b) Acceleration x-direction (train heading direction).

Fig. 7. Examples of raw measurements and LPF results.

train in this paper, noise affects every IMU data largely in x, y, z-directions. Noises in IMU have low and high frequency spectrum, and impulse components are also included. It is considered that noise components at the high frequency are from unstable power source, vibration of train, and passengers' movements. In particular, impulse and low frequency noises, which come from impacts when the train passes connection points of rails, seem to effect mainly on the IMU data. Fig. 6 describes a normalized amplitude of fast Fourier transform (FFT) results of the gyroscope z-direction (yaw-rate) and the accelerometer x-direction (train heading direction) as examples of IMU data.

The FFT results of gyroscope z-direction and accelerometer x-direction in Fig.6 show that meaningful frequency components are concentrated at the low frequency range; about 0 to 2.5 Hz for gyroscope z-direction and 0 to 0.2 Hz for accelerometer x-direction. Because recorded navigation data is aperiodic, periodic frequency componets are considered as noises. Several peaks over 20 Hz of accelerometer x-direction are considered as noises because high pass filtering with a cutoff frequency of 20 Hz does not provide meaningful navigation results. Thus, low pass filters (LPFs) are applied to remove high-frequency noise componets, and their cutoff frequencies are set to 2.5 Hz for gyroscope z-direction and 0.5 Hz for accelerometer x-direction, respectively.

Raw and filtered measurements are shown in Fig. 7. Noises can be reduced by applying LPF. High frequency noises seem to be reduced to proper level in Fig. 7(a) and 7(b), however, time delay problem has arisen. The time delays are about 0.5s and 2.5s for gyroscope z-direction with a cutoff frequency of 2.5 Hz and accelerometer x-direction with a cutoff frequency of 0.5 Hz, respectively. As the cutoff frequency of the LPF increases, noise reduction performance and time delay decrease, and vice versa.

There are six-degrees of freedom (6-DOF) of the IMU sensor (each gyroscope and accelerometer in x, y, z-directions), so that the time delay makes unexpected nonlinear effects on the final estimation due to time-distorted measurements in every direction. There may be some other filtering techniques to resolve this issue, however, computational complexity of filtering techniques and time delay on real-time navigation system for the next development-phase may increase. Therefore, instead of

using a gyroscope for the direction measurement, GPS heading is considered as an alternative direction measurement. Acceleration in y-direction of the body frame is not considered for the navigation, so that x-direction and z-direction of acceleration measurements are used. An assumption that train movement is considered as a straight movement during small time interval because of small curvatures at the corners for the HST, and it makes those alternatives valid. By applying alternative approaches, the attitude and velocity of the train can be estimated.

4. PERFORMANCE ANALYSIS AND SIMULATION RESULTS

In this section, performance of the HST navigation system is analyzed with real experiment data, which is collected by KRRI. For simulations, the value of design parameters such as the initial state $\mathbf{x}^{(0)}$ and state covariance $\Sigma_{\mathbf{x}^{(0)}}$, system covariance matrix Λ, and measurement covariance matrix $\mathbf{R}$ should be carefully determined. In general, the proposed HST navigation system performs coarse alignment and fine alignment to determine initial values of the design parameters at the static state of the train [27]. The initial position $\mathbf{P}^{(0)}$ can be measured by GPS. The initial velocity $\boldsymbol{V}^{n(0)}$ and attitude $\mathbf{Q}_b^{n(0)}$ are roughly determined in the coarse alignment and accurately estimated in the fine alignment. The bias terms of the accelerometer $\boldsymbol{\nabla}^{(0)}$ and the gyroscope $\boldsymbol{\eta}^{(0)}$ are determined in the fine alignment, too. The system covariance $\boldsymbol{\Lambda}$ is determined based on the IMU sensor specification in Table 2 and by the tuning matrix $\boldsymbol{\Gamma}$. Note that the weighting factors in the tuning matrix should be determined by considering the real field performance of the proposed system, because there are unexpected noise components resulting in correlated errors in practice. The measurement covariance matrix $\mathbf{R}$ can be constructed using the sensor specifications in Table 2.

To evaluate the accuracy of the navigation system, ground truth points are necessary. However, at this development stage, we only have positions of RFID tags on the rails with 300m intervals, which had been precisely measured by Hyundai MnSOFT. Note that, RFID tag positions are used for both measurement and gound truth. When RFID tag positions are used for a sensor measurement, it is assumed that there is a $0.5m$ of 1σ uncertainty due to positioning error and time delay of RFID radio signal. The KRRI is considering more accurate time detection techniques for reducing time delays between RFID reader module and RFID tags after development phase in the near future.

4.1. Graphical results

To evaluate the train navigation system, a number of rail sections (1) to (4) are selected as shown Fig. 2. A Fig. 8 shows navigation results at the tunnel sections (1) and (2).

Table 2. Specifications of sensors.

Sensor	Measurement	Covariance Error ($1\sigma_{(\cdot)}$)
GPS	Position	10[m]
	Velocity	5[m/s]
IMU	Acceleration	Bias: 16[mg] , White-noise: 1.5[mg]
Tachometer	Velocity	10[m/s]
RFID	Position	0.5[m]

The tunnel (1) is about 350m length and has one RFID tag (yellow triangle) inside the tunnel. At the entrance of the tunnel (in Fig. 8(a)), there is a disconnection of GPS (purple circle) because satellite signals are blocked in the tunnel. At the exit of the tunnel, federated (blue square) and map matching (red star) results at the first RFID tag (after the exit) do not follow the rail smoothly, because of unstable GPS outputs (red-dashed circles).

In the tunnel, relatively accurate two measurements (GPS position and velocity) are not updated, so it leads large position errors between RFID tags. Horizontal errors of federated output along with a rail can be corrected by map matching algorithm, however, only longitudinal errors can be corrected by RFID tag. Unfortunately, incorrect GPS time measurement after the exit is unpredictable, thus, virtual RFID tagging time is computed improperly. This problem leads a disconnection of navigation outputs (federated and map matcing) at second RFID tag. Different from the tunnel (1), there is only a disconnection of GPS (without scattering) in the tunnel (2) which is about 580m length and has two RFID tags inside the tunnel, but federated and map matching outputs seem like continuous and correct results. At the exit of the tunnel (2), federated results and map matching results are smoothly connected as same as at the entrance.

Fig. 9(a) shows navigation results at the tunnel (3) section. Tunnel (3) is about 240m length and has one RFID tag inside the tunnel. As same as tunnel (2), there is only a disconnection of GPS output in the tunnel, so federated and map matching outputs are continuously and correctly connected. But after the exit of the tunnel, improper GPS outputs make the federated results and map matching results to be slightly concentrated at the exit. This concentration leads position errors of federated and map matching outputs. Different from the tunnels, GPS, federated, and map matching outputs in the open-sky are computed similarly at the same time step.

4.2. Numerical results

Fig. 10 shows 2-dimenstional position errors measured from 94 RFID tags. The first number of RFID tag starts from near Jeongeup station, so that the last number of the RFID tag is nearby Iksan station. Among 94 RFID tags, index number 11 is installed in the tunnel (1), index number 21 and 22 are installed in tunnel (2), index number 82

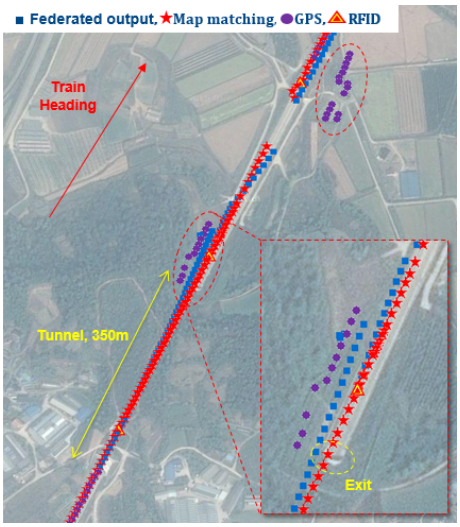

(a) Tunnel (1)

(b) Tunnel (2)

Fig. 8. Navigation results at GPS outages.

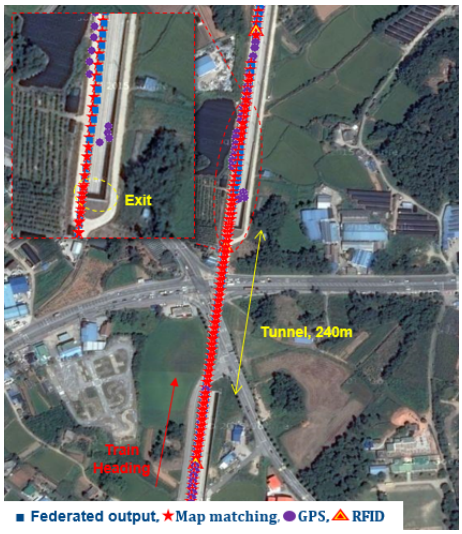

(a) Tunnel (3)

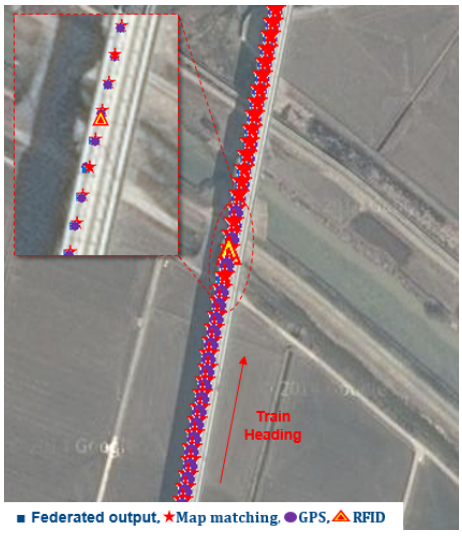

(b) Open-sky

Fig. 9. Navigation results at GPS outage and open-sky.

is installed in the tunnel (3), and the others are installed in the open-sky area.

At the tunnel (1) section, large position errors are seen at tag index 11, 12, and 13, as shown in Fig. 10 (also, refer the map: Fig. 8(a)). These errors are from two sources. At first, GPS degradation leads degradation of final estimation results in the tunnel or shortly after the exit.

Additionally, the information of RFID tagging time is not perfectly synchronized with the true time when the train passes over the RFID tag because it is a virtual tagging data generated from the GPS time. Accurate GPS time is not available at the GPS outages. This degradation naturally be removed after adjustment GPS settings and complete development of RFID module.

Tunnel (2) section (tag index 21, 22, 23) has small positioning errors, as shown in Fig. 10 (also, refer the map: Fig. 8(b)). Different from the tunnel (1), the estimated result from entire section of the tunnel (2) is considered as proper and has very small errors. The reason of small

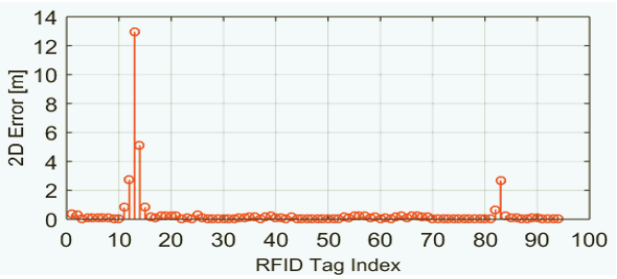

Fig. 10. 2D errors at the RFID tags.

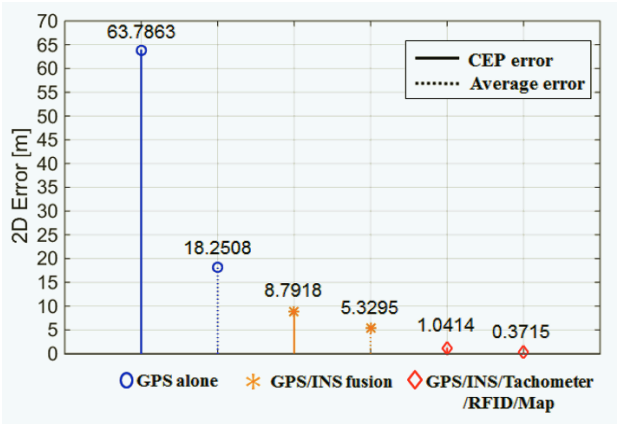

Fig. 11. Comparison of 2D errors with respect to navigation systems.

errors is that from the Fig. 8(b), there are no improper GPS results excepting just disconnection. Also, the tagging time from the virtual RFID data seems to be synchronized quite well with the true time when the train passes over the RFID tag, even at the GPS outages. Numerical errors in tunnel (3) section (tag index 82, 83) are small compared to those in tunnel (1).

Fig. 11 shows navigation errors in circular error probability (CEP) and average with respect to the navigation systems. GPS alone and GPS/INS fusion systems which are considered as conventional navigation systems are compared with the Korean high-speed train navigation system employing GPS/INS/Tachometer/RFID/Map fusion system. In case of GPS alone in this testbed, 2-dimensional errors in CEP and average are the worst among navigation systems. The errors of the GPS alone are mainly from GPS outages since there are no information from other sensor to correct the error. Accuracy of the GPS/INS fusion system is increased about seven times in CEP error and three times in average error compared to GPS alone case. An INS corrects the error from GPS degraded environments such as GPS outages and lack of the number of satellite signals. The Korean HST navigation system has much better positioning accuracy compared to the conventional navigation systems. It provides better positioning accuracy about sixty times in both CEP and average errors compared to the GPS alone, and about eight times and fourteen times in CEP and average errors compared to the GPS/INS fusion system. Since the RFID provides very accurate position information, it plays an important role in GPS outages. Also, map matching algorithm corrects the error components of the perpendicular direction of the train heading.

5. CONCLUSION

This paper realizes and demonstrates that the navigation system of the Korean high-speed train achieves its sub-meter positioning accuracy using real navigation data. The navigation system employs a multi-sensor fusion technique which integrates GPS, INS, tachometer, and RFID sensors utilizing federated Kalman filters with feedback scheme. In real railway environments, almost sensor measurements have unexpected large noise components. To avoid heavy computational burden on hardware, outlier rejection and digital filtering techniques, and algorithm modification for sensors before the local filters. The performance of the navigation system is analyzed with respect to rail sections on the testbed. In open-sky condition, the navigation system has within 1-meter positioning accuracy, but in GPS outages such as tunnels, positioning errors increase. The CEP and average errors of the navigation system employing multi-sensor fusion and map mapping algorithm satisfy a target 1-meter positioning accuracy. Therefore, the HST navigation system employing multi-sensor data fusion and map matching algorithm outperforms conventional navigation systems such as GPS only or GPS/INS fusion systems.

REFERENCES

[1] R. Mázl and L. Přeučil, "Sensor data fusion for inertial navigation of trains in GPS-dark areas," *Proc. of the IEEE Intelli. Veh. Symp.*, pp. 345-350, 2003.

[2] B. Allotta, P. D'Admio, M. Malvezzi, L. Pugi, A. Ridolfi, and G. Vettoti, "A localization algorithm for railway vehicles," *Proc. of the IEEE Int. Instrument. and Meas. Tech. Conf. (I2MTC)*, pp. 681-686, 2015.

[3] S.-H. Kong, "Fast multi-satellite ML acquisition for A-GPS," *IEEE Trans. on Wire. Comm.*, vol. 13, No. 9, pp. 4935-4946, Sep. 2014.

[4] S. G. Park, H. C. Jeong, J. W. Kim, D.-H. Hwang, and S. J. Lee, "Magnetic compass fault detection method for GPS/INS/magnetic compass integrated navigation systems," *Int. J. Contr., Autom. and Syst.*, vol. 9, No. 2, pp. 276-284, 2011.

[5] C. W. Jeon, G.-I. Jee, and G. Lachapelle, "Development of a sequential algorithm for a GNSS-based multi-sensor vehicle navigation system," *Int. J. Contr., Autom. and Syst.*, vol. 2, No. 2, pp. 165-170, 2004.

[6] A. Genghi, L. Marradi, L. Martinelli, L. Campa, G. Labbiento, J. Cianci, G. Venturi, G. Gennaro, and M. Tossaint,"The RUNE project: design and demonstration of a GPS/EGNOS-based railway user navigation equipment," *Proc. of ION GPS/GNSS*, pp. 225-237, 2003.

[7] L. Drolet, F. Michaud, and J. Cote, "Adaptable sensor fusion using multiple Kalman filters," *Proc. of the IEEE/RSJ Inter. Conf.* vol. 2, 2000.

[8] J. Z. Sasiadek and P. Hartana, "Sensor data fusion using Kalman filter," *Proc. of the IEEE/FUSION 2000. 3rd Inter. Conf.*, vol. 2, 2000.

[9] Z. Wei, S. Ma, Z. Hua, H. Jia, and Z. Zhao, "Train integrated positioning method based on GPS/INS/RFID,"

Proc. of the IEEE 35th Control Conference (CCC), Chinese, 2016.

[10] S. H. You, J. M. Pak, C. K. Ahn, P. Shi, and M. T. Lim, "Unbiased finite-memory digital phase-locked loop," *IEEE Trans. on Circuits and Systems-II*, vol. 63, No. 8, pp. 798-802, Aug. 2016. [click]

[11] B. Ristic and S. Arulampalam, *Beyond the Kalman Filter: Particle Filters for Tracking Applications*, Artech House, 2004.

[12] J. M. Pak, C. K. Ahn, Y. S. Shmaliy, P. Shi, and M. T. Lim, "Switching extensible FIR filter bank for adaptive horizon state estimation with application," *IEEE Trans. on Control Systems Tech.*, vol. 24, No. 3, pp. 1052-1058, May 2016. [click]

[13] D. Simon and Y. S. Shmaliy, "Unified forms for Kalman and finite impulse response filtering and smoothing," *Automatica*, vol. 49, no. 6, pp. 1892-1899, Jun. 2013. [click]

[14] W. H. Kwon and S. H. Han, *Receding Horizon Control: Model Predictive Control for State Models*, Springer-Verlag, London, U.K., 2005.

[15] S. Yin and Z. Huang, "Performance monitoring for vehicle suspension system via fuzzy positivistic C-means clustering based on accelerometer measurements," *IEEE Trans. on Mecha.*, vol. 20, no. 5, pp. 2613-2620, Oct. 2015. [click]

[16] S. Feng, W. Y. Ochieng, D. Walsh, and R. Ioannides, "A measurement domain receiver autonomous integrity monitoring algorithm," *GPS Solutions*, vol. 10, no. 2, pp. 85-96, May 2006. [click]

[17] T. Wartzek, B. Eilebrecht, J. Lem, H. J. Lindner, S. Leonhardt, and M. Walter, "ECG on the road: robust and unobtrusive estimation of heart rate," *IEEE Trans. on Bio. Engine.*, vol. 58, no. 11, pp. 3112-3120, 2011. [click]

[18] W. Qiuping, G. Zhongyu, and W. Dejun, "An adaptive information fusion method to vehicle integrated navigation," *Proc. IEEE PLANS*, Palm Springs, CA, USA, Apr. 2002, pp. 248-253.

[19] K. Kim, S.-H. Kong, and S. Y. Jeon, "Slip and slide detection and adaptive information sharing algorithms for high-speed train navigation systems," *IEEE Trans. on Intelli. Transp. Sys.*, vol. 16, no. 6, pp. 3193-3203, Dec. 2015. [click]

[20] K. Kim, S. Seol, and S.-H. Kong, "High-speed train navigation system based on multi-sensor data fusion and map matching algorithm," *Int. J. Contr., Autom. and Syst.*, vol. 13, No. 3, pp. 503-512, 2015. [click]

[21] T.-G. Lee, "Centralized Kalman filter with adaptive measurement fusion: its application to a GPS/SDINS integration system with an additional sensor," *Int. J. Contr., Autom. and Syst.*, vol. 1, No. 4, pp. 444-452, 2003.

[22] K. C. Chang, R. K. Saha, and Y. Bar-Shalom, "On optimal track-to-track fusion," *IEEE Trans. Aerosp. Electron. Syst.*, vol. 33, no. 4, pp. 1271-1276, Oct. 1997. [click]

[23] M. Mosallaei, K. Salahshoor, and M. R. Bayat, "Process fault detection and diagnosis by synchronous and asynchronous decentralized Kalman filtering using state-vector fusion technique," *Proc. of the ISSNIP 3rd Int. Conf.*, pp. 3-6, Dec. 2007.

[24] H. Zhang, J. Rong, and X. Zhong, "Research of the INS/GPS integrated navigation system for high speed trains," *Proc. of the IEEE 9th ICYCS*, pp. 1659-1663, Nov. 2008.

[25] G. Schänzer, U. Schneider, and J. Troelsen, "The challenges of using satellite navigation systems for high precision railway positioning," *Proc. of 7th conf. on Compu. in Railways VII*, pp. 1281-1290, 2000.

[26] T. Wang, J. Qiu, S. Fu, and W. Ji, "Distributed fuzzy H∞ filtering for nonlinear multirate networked double-layer industrial processes," *IEEE Trans. Indust. Electron.*, vol. 64, no. 6, pp. 5203-5211, Jun. 2017. [click]

[27] D. H. Titterton and J. L. Weston, *Strapdown Inertial Navigation Technology*, Second edition, Institution of Engineering and Technology, 2004.

[28] N. A. Carlson, "Federated square root filter for decentralized parallel processes," *IEEE Trans. Aerosp. Electron. Syst.*, vol. 26, no. 3, pp. 517-525, May 1990. [click]

[29] L. Serrano, D. Kim, R. B. Langley, K. Itani, and M. Ueno, "A GPS velocity sensor: how accurate can it be? - A first look," *Proc. of ION/NTM*, pp. 875-885, Jan. 2004.

[30] H. Ferdowsi, S. Jagannathan, and M. Zawodniok, "An online outlier identification and removal scheme for improving fault detection performance," *IEEE Trans. on Neural Networks and Learning Systems*, vol. 25, no. 5, pp. 908-919, 2014. [click]

[31] "FFFIS for Eurobalise," UNISIG, SUBSET-036, Issue. 3.0.0, Feb. 24, 2012.

Hyunwoo Ko received the B.S. degree in Mechanical and Control Engineering from Handong Global University, Pohang, Korea, in 2014 and the M.S. degree at the CCS Graduate School for Green Transportation in the Korea Advanced Institute of Science and Technology (KAIST), Daejeon, Korea, in 2016.

Youngbo Shim received the B.S. and M.S. degrees in Electronics Engineering from Chungbuk National University, Cheongju, Korea, in 2014 and 2016, respectively. Since 2016, he is with the Korea Advanced Institute of Science and Technology (KAIST), where he is currently a Researcher at the CCS graduate school of green transportation.

Seung-Hyun Kong received his B.S. degree in Electronics Engineering from Sogang University, Korea, in 1992, an M.S. degree in Electrical Engineering from Polytechnic University (merged to NYU), New York, in 1994, and a Ph.D. degree in Aeronautics and Astronautics from Stanford University, CA, in Jan. 2006. From 1997 to 2004, he was with Samsung Electronics Inc. and Nexpilot Inc., both in Korea, where he worked on developing wireless communication system standards and mobile positioning technologies. In 2006 and from 2007 to 2009, he was a staff engineer at Polaris Wireless Inc., Santa Clara, and at Qualcomm Inc. (Corp. R&D), San Diego, respectively, where his research focus was on Assisted-GNSS and wireless positioning technologies. Since 2010, he is with Korea Advanced Institute of Science and Technology (KAIST), where he is currently an associate professor at the CCS Graduate School of Green Transportation. He is an Editor of IET, Radar, Sonar and Navigation, and an Associate Editor of IEEE transactions on ITS and IEEE Access. His research interests include next generation GNSS, advanced sensing and signal processing for navigation systems, and vehicular communication systems.